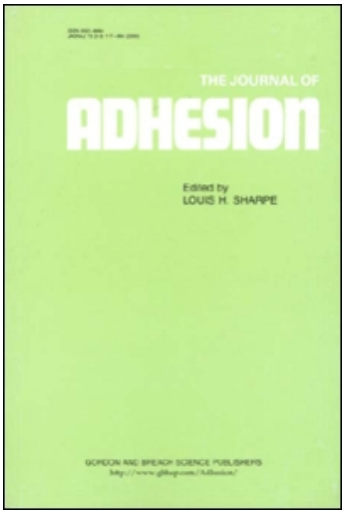

The Journal of Adhesion
Publication details, including instructions for authors and subscription information:
http://www.informaworld.com/smpp/title~content=t713453635

Effect of Adherend Thickness and Mixed Mode Loading on Debond Growth in Adhesively Bonded Composite Joints

P. D. Mangalgiri[a]; W. S. Johnson[a]; R. A. Everett Jr.[a]
[a] NASA Langley Research Center, Hampton, Virginia

To cite this Article Mangalgiri, P. D. , Johnson, W. S. and Everett Jr., R. A.(1987) 'Effect of Adherend Thickness and Mixed Mode Loading on Debond Growth in Adhesively Bonded Composite Joints', The Journal of Adhesion, 23: 4, 263 — 288
To link to this Article: DOI: 10.1080/00218468708075410
URL: http://dx.doi.org/10.1080/00218468708075410

J. Adhesion, 1987, Vol. 23, pp. 263–288
Photocopying permitted by license only

Printed in the United Kingdom

Effect of Adherend Thickness and Mixed Mode Loading on Debond Growth in Adhesively Bonded Composite Joints†

P. D. MANGALGIRI, W. S. JOHNSON and R. A. EVERETT, JR.

NASA Langley Research Center, Hampton, Virginia

(Received October 20, 1986)

Symmetric and unsymmetric double cantilever beam (DCB) specimens were tested and analyzed to assess the effect of (1) adherend thickness and (2) a predominantly mode I mixed mode loading on cyclic debond growth and static fracture toughness. The specimens were made of unidirectional composite (T300/5208) adherends bonded together with EC3445 structural adhesive. The thickness was 8, 16 or 24 plies. The experimental results indicated that the static fracture toughness increases and the cyclic debond growth rate decreases with increasing adherend thickness. This behavior was related to the length of the plastic zone ahead of the debond tip. For the symmetric DCB specimens, it was further found that displacement control tests resulted in higher debond growth rates than did load control tests. While the symmetric DCB tests always resulted in cohesive failures in the bondline, the unsymmetric DCB tests resulted in the debond growing into the thinner adherend and the damage progressing as delamination in that adherend. This behavior resulted in much lower fracture toughness and damage growth rates than found in the symmetric DCB tests.

KEY WORDS Adhesive joints; composites; double cantilever beam; fatigue; fracture toughness; mixed mode.

1 INTRODUCTION

Fiber reinforced composite materials offer significant advantages in terms of strength-to-weight and stiffness-to-weight ratios in con-

† Presented at the Tenth Annual Meeting of The Adhesion Society, Inc., Williamsburg, Virginia, U.S.A., February 22–27, 1987.

structing aerospace structures. However, their effective use may be limited by the efficiency and reliability of the joining methods used in the construction. Mechanical fastener holes weaken the composites significantly, and some of the advantage in weight saving may be lost in strengthening these holes. Adhesive bonding offers a viable alternative with a number of potential advantages such as (1) higher joint efficiency, (2) no strength degradation of basic composite, (3) less expensive and simpler fabrication techniques, and (4) lower part count and maintenance cost. Currently, most aerospace industries are hesitant to use adhesive bonding in joining primary structures. This is due partly to the lack of understanding of adhesive bond behavior, particularly under conditions of repeated loading over an extended period of time. The objective of the present paper is to contribute toward a better understanding of the adhesive debond growth behavior by using fracture mechanics concepts.

Earlier, the fracture mechanics concept of strain energy release rate was used to model the debond growth under cyclic loading by Roderick, Everett and Crews[1] while studying composite-to-metal joints. The rate of debond growth was correlated to the total strain energy release rate. The total strain energy release rate, G_T, in adhesive debonding may be composed of three components: opening mode G_I, sliding mode G_{II}, and tearing mode G_{III}. However, in most cases of practical adhesive joints, the strain energy release rate is composed of only G_I and G_{II}. Two types of specimens have been commonly used in the past for debond studies: (1) Double Cantilever Beam (DCB) specimen to study pure mode I behavior and (2) Cracked Lap Shear (CLS) specimen to study mixed mode I and II behavior with G_I/G_{II} in the range of 0.25–0.5.[2–6] Various investigators of the debond behavior have used different kinds of adherend and adhesive thicknesses in DCB specimens in their studies. Whereas considerable attention has been devoted in the past to the influence of the bondline thickness, little information exists on the influence of adherend thickness. A change in adherend thickness would result in change of stress state ahead of the debond tip, and it is of interest to examine how this would influence the debond growth behavior and static fracture toughness.

Mall, Johnson, and Everett[2] studied the debond growth in CLS specimens with quasi-isotropic graphite-epoxy adherends and two

adhesives. They found that even though the debond grew in mixed mode ($0.25 < G_I/G_{II} < 0.38$), the debond growth rate correlated better with the total strain energy release rate than with either G_I or G_{II} alone. Mall and Johnson[3] further examined this correlation with experiments on DCB (mode I) specimens and found that the correlation of debond growth rate with $G_I = G_T$ in DCB specimens agreed with that of G_T in CLS specimens. These experiments lead to an hypothesis that the total strain energy release rate is the governing parameter for the debond growth in adhesive joints. The practical significance of such a finding is that it will simplify design and analysis procedures, since total strain energy release rate is much easier to determine than the individual components. These studies on the mixed mode behavior than the individual components. These studies on the mixed mode behavior have demonstrated the validity of the hypothesis under predominantly mode II conditions existing in CLS specimens ($G_I/G_{II} < 0.38$) and the pure mode I conditions in the DCB specimen. It needs to be verified in other cases of mixed mode loading.

The purpose of this paper is twofold: (1) to investigate the influence of adherend thickness on debond growth under static and fatigue loading and (2) to study debond growth in mixed mode under a predominantly mode I loading ($G_I/G_{II} > 5.6$). Experiments were conducted on DCB specimens of various thicknesses. Mixed mode was introduced by making the two adherends of different thicknesses thus making the specimen unsymmetric. The influence of various parameters is ascertained by measuring fracture toughness (critical strain energy release rate) in static loading and cyclic debond growth rates in fatigue loading. Analysis by the Finite Element Method (FEM) was used to determine individual components of strain energy release rate and to interpret other results.

2 EXPERIMENTS

2.1 Specimen, materials and preparation

The double cantilever beam specimen as shown in Figure 1 was used in the present study. When the two adherends are of equal thickness the specimen is "symmetric" and has pure mode I

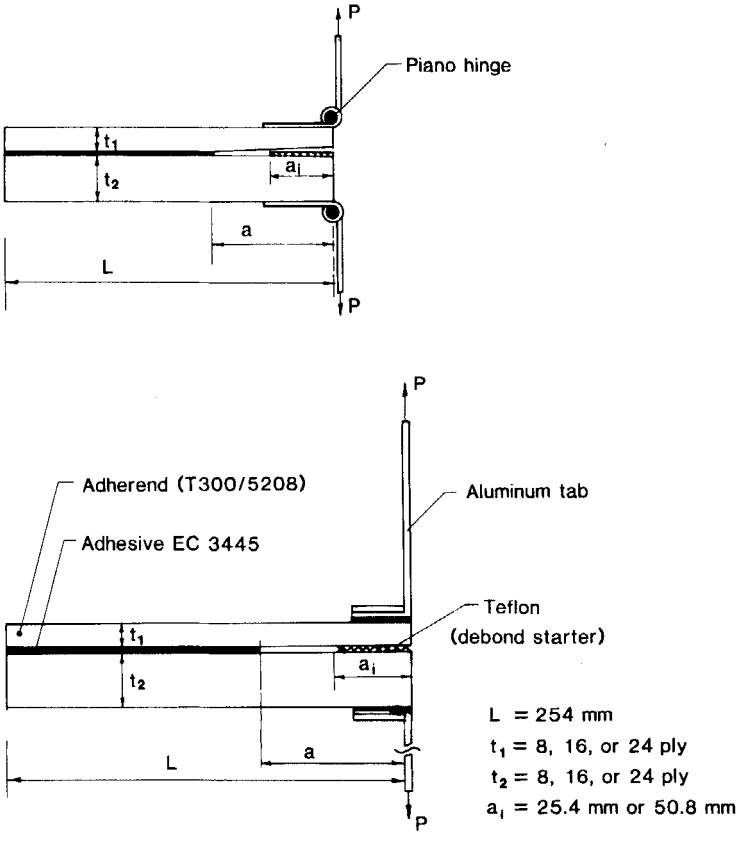

FIGURE 1 Specimen geometry and nomenclature.

behavior under the loads shown in the figure. By making one adherend thicker than the other, the specimen can be made "unsymmetric" introducing a mixed mode behavior under the same loading conditions while maintaining a predominantly mode I situation. For the present work, adherends were made of unidirectional graphite-epoxy (T300/5208)† composite and the adhesive used was EC3445,‡ a thermosetting paste adhesive with a cure temperature of 121°C. The material properties of the undirectional

† T300/5208 supplied by Hexcel Corp., California, USA.
‡ EC3445 is manufactured by 3-M Corp., Minnesota, USA.

graphite-epoxy adherends were obtained from Ref. 7. These are presented in Table I. The EC3445 adhesive is the paste version of the AF-55 adhesive film; therefore, the Young's modulus of EC3445 was calculated from the data on AF-55 by assuming the adhesive to be an isotropic material with Poisson's ratio of 0.4. These properties taken from Ref. 2 are also presented in Table I.

Three panels, one each of 8, 16, and 24 plies thickness, of unidirectional graphite-epoxy (T300/5208) were first fabricated. Strips of width 25.4 mm (1.0 in) and length 254 mm (10.0 in) were cut from these panels. Symmetric (8-ply to 8-ply, 16-ply to 16-ply, 24-ply to 24-ply) and unsymmetric (8-ply to 16-ply, 8-ply to 24-ply, 16-ply to 24-ply) DCB specimens were fabricated by bonding two of these strips together with EC3445 adhesive using a conventional secondary bonding procedure. Nominal adhesive thickness was maintained at 0.10 mm (0.004 in) by random sprinkling of a small volume fraction (less than 0.1%) of glass beads of 0.10 mm diameter. An initial debond was introduced by inserting a Teflon® film 0.0125 mm (0.0005 in) thick during the bonding procedure. The length of this initial debond was kept 25.4 mm (1.0 in) for thinner specimens and 50.8 mm (2.0 in) for thicker specimens to allow similar loading ranges. Initially, two aluminum tabs 0.5 mm thick were bonded at the ends of DCB specimens (see Figure 1a) to facilitate application of load. A room temperature cure adhesive was used for bonding these tabs. These tabs debonded in certain cases and also introduced additional constraints at the ends. Subsequently, steel hinges were employed instead of the aluminum tabs (see Figure 1b) which led to a very satisfactory performance.

TABLE I
Elastic properties of adherend and adhesive materials

	E_1 (GPa)	E_2 (GPa)	G_{12} (GPa)	υ_{12}
1. Adherend T300/5208 Undirectional	131.0	13.0	6.4	0.34
2. Adhesive EC3445	1.81	1.81	0.65	0.40

Virtually all the results reported herein are from specimens using the steel hinges.

2.2 Testing procedure

The objective of the test program was to determine two characteristics: (1) the critical strain energy release rate in static loading and (2) the debond growth rate under cyclic fatigue loading. Both the static and fatigue tests were carried out in the same set-up as described below.

All specimens were tested in a closed-loop electro-hydraulic test machine specially equipped to measure and control small testing loads (less than 225 N or 50 lbs). All static tests and most fatigue tests were performed in the displacement control mode. For fatigue tests, cyclic loads were applied in both load and displacement control mode to ascertain the difference in the two procedures. In such tests, it was found convenient to apply load control at smaller crack-lengths (when loads are comparatively large and displacements small) and displacement control at larger crack-lengths (when loads are comparatively small and displacements large). Both edges of the specimen were coated with white brittle fluid (in this case typewriter correction fluid) to aid in visually locating the debond tip. Fine visible scale marks were put on the edges of the specimen to aid in the measurement. The debond tip was observed through microscopes having a magnification factor of 20. The magnification and the fine scale helped to locate the debond tip within 0.25 mm (0.01 in) accuracy. The debond length was observed on both sides of the specimen. The mean difference in readings on the two sides was less than 5%, and the maximum difference was 15% of the debond length (12 mm over a width of 25.4 mm). The debond length was taken as the average of readings on both sides of the specimen.

During the static fracture toughness tests the crosshead speeds were adjusted to obtain strain rates normal to the crack surface in the adhesive 0.1 mm ahead of the crack tip in the range of 0.001–0.0025 per minute for each test. Since the stresses at the crack tip in a DCB specimen are inversely proportional to the square of the length, the crosshead speeds were increased as the

square of the debond length to achieve nearly the same crack tip strain rate for all tests. As the displacement was applied, the onset of growth resulted in a deviation from linearity in the load-displacement curve. After the onset of growth was observed, the specimen was unloaded at the same crosshead speeds.

For fatigue tests, cyclic loads were applied at a frequency of 3 Hz. This frequency was chosen to facilitate comparison with the earlier data.[2,3] Constant amplitude cyclic loading was applied with the ratio of minimum to maximum load (or displacement) of 0.1. In the load control mode (constant load amplitude), the debond growth rate increases as the debond grows whereas in the displacement control mode (constant displacement amplitude) the growth rate decreases with the growth of the debond. Therefore, in the load control mode cyclic load amplitude was chosen to give very slow growth rates (1-5 nm/cycle) to start with and maintained until the debond growth rates were too fast to be accurately measured or controlled (approximately 0.05 mm/cycle). The load amplitude was then reduced for a further increment of the debond growth starting with the slow growth rate. On the other hand, in the displacement control mode cyclic displacement amplitude was chosen to give high but controllable and measurable debond growth rate (approximately 0.05 mm/cycle) to start with and was maintained until the growth rate became very slow (1-5 nm/cycle). The displacement amplitude was then increased for a further increment of the debond growth starting with the high growth rate. Static tests were usually conducted at the changeover from one amplitude to the other. This also provided the required sharp crack for the static tests. Debond length (a), number of load cycles (N), and the applied load (P) or displacement (v) were monitored throughout the tests. The crack growth data taken immediately after a static fracture test was not used in the calculation of the crack growth rate. Load-displacement records were taken at suitable intervals of debond length.

The values of the strain energy release rates were calculated from the recorded load displacement relationship and the applied loads. The record of debond lengths at various numbers of cycles provided data for the calculation of the debond growth rate da/dN. The details of the computational procedures are given in the next section.

3 ANALYSIS

As reported in the earlier section, load-displacement records were obtained at several debond lengths. To obtain the strain energy release rate, the compliance of the specimen was calculated at each debond length from the load-displacement record. The total strain energy release rate (G_T) is related to the compliance (C) by the relation

$$G_T = 0.5(P^2/b)\, dC/da \tag{1}$$

A simple strength of materials analysis derived from linear beam theory for the symmetric DCB specimen[3,9] gives the compliance as

$$C = 8a^3/bEt^3 \tag{2}$$

for plane stress conditions where E is taken as the longitudinal modulus.[8] This expression is valid as long as the modulus is taken as the apparent modulus as discussed by Ashizawa.[10] Ashizawa has also presented correction factors for the flexural modulus. The unsymmetric DCB specimen can also be analyzed in a similar fashion by treating each half as a cantilever beam having different flexural stiffnesses. Since the specimen is unsymmetric, it will tend to rotate somewhat under load (*i.e.*, the bondline will not remain perfectly horizontal). As long as this rotation is rather small, the compliance C is then given by

$$C = 4(a^3/bE)(1/t_1^3 + 1/t_2^3). \tag{3}$$

The compliance given by Eq. (3) is in good agreement with finite element analysis of the specimen. As seen from the Eqs. (2, 3), the value of C is very sensitive to the measurements of thickness and crack length. Moreover, correction factors need to be applied to the modulus E as shown by Ashizawa.[10] Hence, these equations cannot be directly used to analyze experimental data. Since, in general, the compliance is proportional to the cube of the crack length a, a relation of

$$C = A(a)^3 \tag{4}$$

was fitted through the experimental data points by the method of least squares. The total strain energy release rate is then calculated using Eq. (1).

A finite element analysis using GAMNAS, a program developed at NASA,[11] was also conducted for comparison with the beam theory and to calculate the stress state ahead of the debond tip. The virtual crack closure technique was used to calculate the strain energy release rates. Plane strain conditions were assumed to exist in the bondline. The finite element mesh was refined to the extent that further refinement resulted in essentially the same results. The GAMNAS program was also used to assess the effect of the adhesive bondline plasticity on the specimen load-displacement behavior. The adhesive was modeled as a bi-linear elastic–plastic material with a yield strength of 32 MPa. The elastic modulus was 1.81 GPa and the plastic modulus was taken as 0.40 GPa. Only the 24- to 24-ply specimen was analyzed because it showed the greatest effect of loading mode on resulting debond growth rate.

4 RESULTS AND DISCUSSION

In this section the data obtained in the static and fatigue tests are analyzed and the results are discussed. First, the determination of basic parameters, namely compliance, strain energy release rate, and debond growth rates, is discussed. These and other data are then used to discuss various aspects such as the influence of load or displacement control mode, the influence of adherend thickness, and the influence of mixed mode on static and fatigue debond growth.

4.1 Determination of basic parameters

The static tests yielded the compliance data and the critical loads. The relation of Eq. (4) was found to fit very well with the experimental data as shown in Figure 2. Data points are shown for a symmetric 24-ply to 24-ply and unsymmetric 24-ply to 8-ply specimens. Values obtained by FEM analysis are also shown in the figure. Although the FEM values show the cubic variation, they differ from the experimental values by as much as 12%. As noted earlier in the section on analysis, the compliance values are very sensitive to the measurement of thickness and debond length. In practice, the thickness of the specimen was not uniform. Other

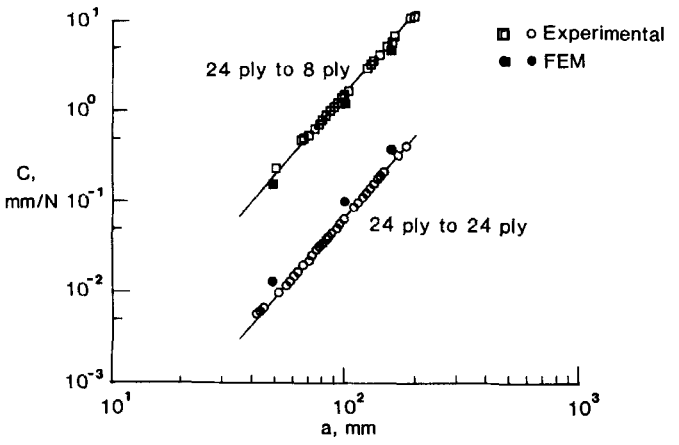

FIGURE 2 Relation between compliance C and debond length a, for symmetric and unsymmetric DCB specimens.

factors such as experimental errors in load control and compliance measurements could also contribute to this rather small difference between the analysis and experiment.

Linear FEM analysis with the debond placed in the middle of the adhesive yielded compliance values which showed the cubic variation with respect to a. Further, the geometric nonlinear analysis did not indicate any significant difference in either the compliance or the computed G values from the linear analysis. The maximum difference in G_T was less than 3% for a debond length of 100 mm under maximum experimental load. A significant outcome of the FEM analysis was the individual values of G_I and G_{II} for the unsymmetric DCB. Maximum G_{II} contribution was in the most

TABLE II
Mixed mode ratios for the unsymmetric DCB specimens

Configuration	G_I/G_{II}	G_I/G_T
8-ply to 24-ply	5.67	0.85
8-ply to 16-ply	11.50	0.92
16-ply to 24-ply	24.00	0.96
Symmetric	—	1.00

unsymmetric case (24-ply to 8-ply) and was about 15% of G_T. The G_I/G_{II} ratios for the unsymmetric DCB specimens are shown in Table II. The analyses did not show any significant variation in G_I/G_{II} with either the load or the debond length.

The fatigue tests yielded the debond growth data. The values of the operating strain energy release rate (G_T) at the center of the debond increment were calculated from the compliance relationship, Eq. (4), obtained by a least squares fit of the compliance data. Plots of da/dN *vs.* G_T were made and a least squares fit was used to obtain the constants c and n in the relationship

$$da/dN = cG_T^n. \tag{5}$$

This equation was found to fit well for all data sets. Table III gives the values of parameters c and n obtained for the various cases. The results obtained are discussed below.

TABLE III
Crack growth rate parameters c and n in the relation $da/dN = c\,(G_T)^n$ m/cycle with DG in J/m^2

Configuration t_1 Plies	t_2 Plies	Control mode	c	n	No. of data points
		Load	3.381E-19	4.801	36
8	8	Disp	6.124E-20	5.083	36
		Both	2.658E-19	4.831	72
		Load	3.528E-19	4.980	32
16	16	Disp	3.207E-23	6.282	42
		Both	5.080E-24	6.495	74
		Load	1.368E-21	5.598	19
24	24	Disp	1.737E-24	7.165	36
		Both	8.009E-20	5.157	55
8	16[a]	Disp	4.076E-21	6.178	70
8	24[b]	Disp	8.601E-38	13.815	62

[a] Failure at the interface/Delamination in the adherend.
[b] Delamination in the adherend.

4.2 Influence of load/displacement control mode

Figures 3a, 3b, and 3c show the debond growth rate with the cyclic G values for symmetric DCB specimens with 8-, 16- and 24-ply adherends, respectively. The filled symbols and the solid lines refer to the data obtained in the displacement control mode whereas the open symbols and the broken lines refer to those in load control mode. If apparent threshold data were present (this applies to the data at growth rates below 10^{-10} m/cycle that tend toward a vertical line), the threshold related data points were not used in the determination of best fit line to the debond growth rate data. For example, the seven open symbols below the growth rate of 10^{-10} in Figure 3a were not used to determine the best fit line. The control mode had little if any effect on the cyclic debond growth behavior in the case of the thin (8-ply) adherends, Figure 3a, but the effect became more significant as the adherends became thicker as shown by the data for the 16-ply and 24-ply cases in Figure 3b and 3c, respectively. Where the effect was significant, the displacement control mode resulted in a higher debond growth rate for the same

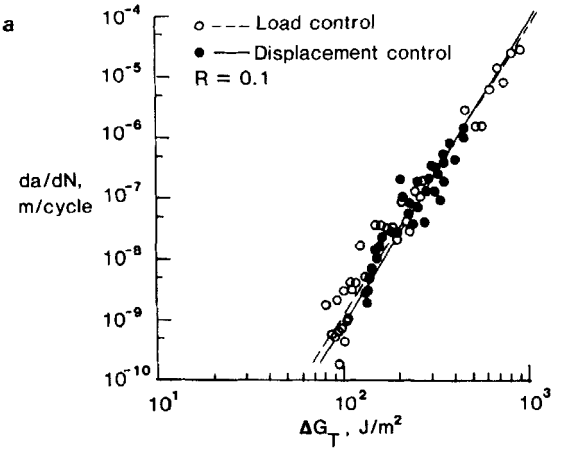

FIGURE 3 (a) Effect of load/displacement control mode on debond growth rate in symmetric DCB specimens (8-ply to 8-ply). (b) Effect of load/displacement control mode on debond growth rate in symmetric DCB specimens (16-ply to 16-ply). (c) Effect of load/displacement control mode on debond growth rate in symmetric DCB specimens (24-ply to 24-ply).

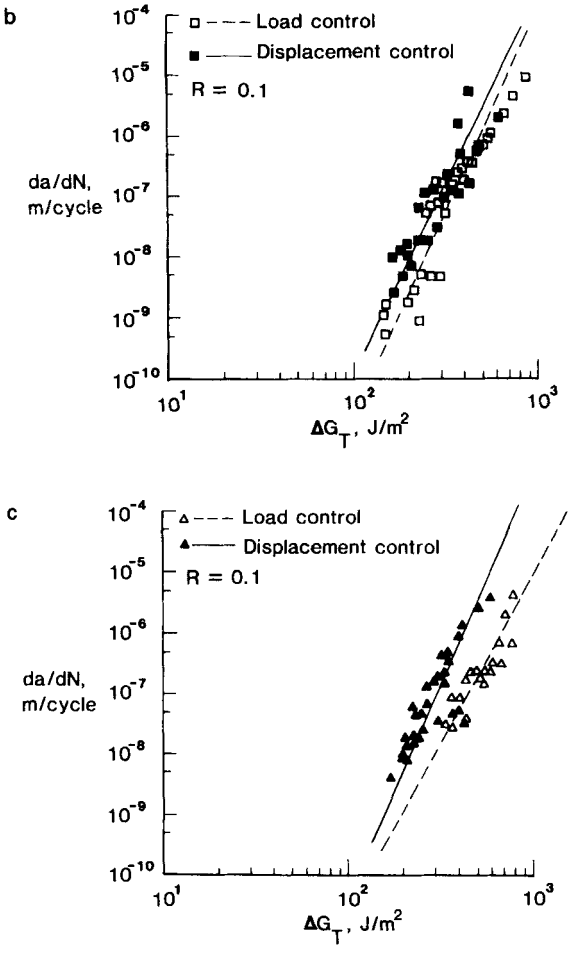

FIGURE 3 (*continued*)

operating strain energy release rate. This is consistent with the observation made earlier by Mall and Johnson.[3]

The G_I values are calculated based on elastic material response; however, structural adhesives are both elastic–plastic and viscoelastic. In the displacement control mode the amount of debond tip opening and the resulting stress distribution ahead of the debond are rather constant for a given applied displacement because the

displacements are controlled by the adherends. However, for the load control mode the debond tip may open further than calculated elastically due to either a plastic or viscoelastic deformation of the adhesive. Therefore, the stress distribution ahead of the debond may increase, resulting in a larger plastic zone. Perhaps this contributes in some way to the reason why the load control tests result in slower crack growth rates.

The finite element analysis of the 24- to 24-ply DCB specimen supported the fact that the specimen would open more under load control with the elastic–plastic adhesive properties than with the purely elastic adhesive properties. The analysis also showed that the displacement controlled tests with the elastic–plastic adhesive required less reactive load than a specimen with an elastic adhesive. However, at an applied G_I level of 480 J/m^2, the differences in the elastic and the elastic–plastic results were far less than one percent. This difference is too small to account for the observed behavior of the adherend is controlling the load-displacement response of the specimen. The plasticity at the crack tip has little influence on the over all specimen stiffness response.

The 24-ply debond growth rate is as much as an order of magnitude less for the load controlled data than for the displacement controlled; or at a given debond growth rate, tests in load control require up to twice the G level. There is at the moment no explanation for this behavior using linear elastic fracture mechanics.

4.3 Influence of adherend thickness

The higher flexural rigidity of the thicker adherends affects the stress distribution ahead of the debond tip. It is of interest to investigate whether this would affect the fracture toughness and debond growth rates.

Figure 4 shows the results obtained in static fracture toughness tests with various symmetric DCB specimens. Two specimens of each type were tested at several debond lengths. The average toughness values and the range of scatter are shown in the figure. The numerals in the parentheses indicate the number of data points. It is observed from the figure that there is an increase in the average value of G_{Ic} as the adherends become thicker. The change in G_{Ic} is more significant from 8-ply to 16-ply than from 16-ply to 24-ply.

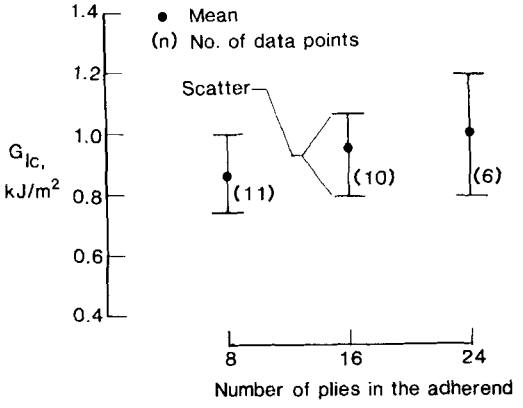

FIGURE 4 Influence of adherend thickness on fracture toughness in symmetric DCB specimens.

However, the change in average G_{Ic} with adherend thickness is of the same order as the scatter in the data, therefore, more information is needed to confirm this trend. Devitt, Schapery, and Bradley[12] have shown a similar thickness-dependent interlaminar fracture toughness in glass/epoxy composites. They tested 8-, 12-, and 16-ply specimens and found the average toughness from five tests to be 831, 873, and 904 J/m^2, respectively. Their data trend is similar to that reported herein.

To study the influence of the adhered thickness on the cyclic debond growth, the data obtained in the fatigue tests are replotted in Figures 5a and 5b. Figure 5a shows the results for the load control mode and Figure 5b for the displacement control mode. The influence of adherend thickness is much less in the displacement control mode than in the load control mode. Further, it appears that the thicker adherends resulted in slower growth rates, particularly for low growth rates. Also, considering the scatter in the individual data sets (Figures 3a, 3b and 3c), it may be observed that the change of the adherend thickness from 16- to 8-ply affected the growth rates more significantly than the change from 24- to 16-ply. Thus, the influence may be more significant for thinner specimens.

In Figure 5b the present results are compared with the results obtained by Mall and Johnson[3] from cracked lap shear and DCB specimens made with the same adhesive and adherend materials.

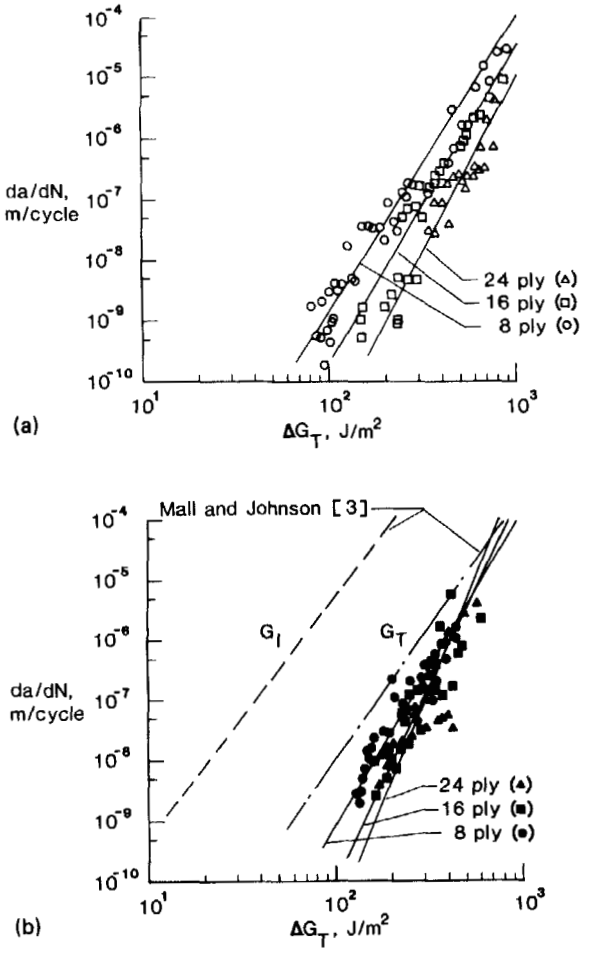

FIGURE 5 (a) Influence of adherend thickness on cyclic debond growth of EC3445 adhesive in symmetric DCB specimens under load control mode. The lines are fitted to the data above 10^{-8} m/cycle. Below 10^{-8} m/cycle debond growth is in the threshold range. (b) Influence of adherend thickness on cyclic debond growth rate in symmetric DCB specimens tested under displacement control mode.

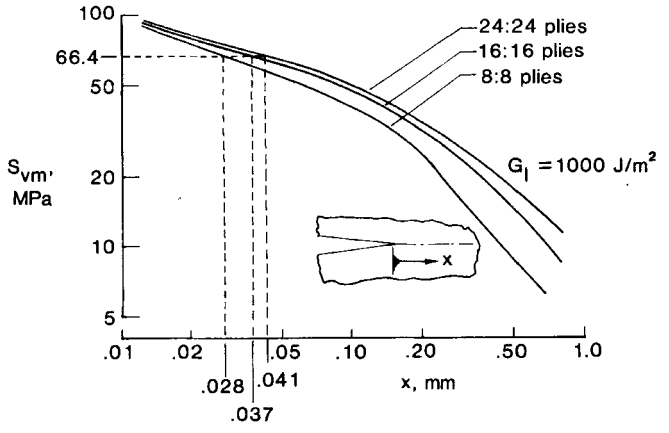

FIGURE 6 Variation of von Mises stress ahead of crack tip for symmetric DCB specimens with various adherend thicknesses and a debond length of 100 mm.

The present data correlate well with the G_T data line but not to the G_I. This supports the previous observations[3] that the debond growth rate of these types of structural adhesives is a function of the total strain energy release rate and not just the mode I component.

An attempt was made to interpret these results in terms of the stress distribution ahead of the crack tip. To facilitate a comparison of the amount of plastic deformation ahead of the crack tip at the same value of the strain energy release rate (irrespective of the loads) in the different specimens, the von Mises's stress is plotted *versus* the distance ahead of the crack tip. The von Mises' stress is defined as

$$S_{vm} = (s_x^2 + s_y^2 + s_z^2 + s_x * s_y + s_y * s_z + s_z * s_x)^{0.5}. \quad (7)$$

Figure 6 shows the variation of S_{vm} ahead of the crack tip of a 100 mm long debond for the three adherend thicknesses tested. Each specimen is loaded so that G is equal to a G_{Ic} of 1000 J/m^2. These data are useful for comparing the relative approximate length of the yield zone at fracture by assuming a value for the adhesive yield stress. The yield shear stress for EC3445 is about 33.2 MPa (4820 psi)† which gives the normal yield stress of 66.4 MPa

† A. V. Pocius, Private Communication, 3M Company, St. Paul, Minnesota 55144-1000, U.S.A.

(9640 psi). Assuming that the distance ahead of the crack tip at which S_{vm} decays to the yield stress is a reasonable approximation of the plastic zone ahead of the crack tip, we observe that the plastic zone size increases with the adherend thickness for the same applied elastic strain energy release rate. The rate of increase in the plastic zone side decreases as the thickness increases (*i.e.*, the change from 24-ply to 16-ply is less than that from 16-ply to 8-ply).

It may be speculated that more energy is dissipated by the plastic deformation of the adhesive as the debond grows in the thicker adherend case than the thinner one. Since the total strain energy release rates are the same for each case, the remaining energy available for crack extension (that is, the total energy minus the energy used for plastic deformation associated with the debond growth) is decreasing with increasing adherend thickness. This leads us to expect that the actual fracture toughness of the thicker adherend may be more than that of the thinner adherend. It also follows that the thicker adherend specimens would show a slower debond growth rate for a given applied G. This agrees with trends of the experimental results in Figures 4 and 5.

Figure 7 shows the normal stress component ahead of the debond tip for each specimen type. These stresses are also from the GAMNAS finite element analysis. Each specimen is loaded such that G_I is equal to 39 J/m^2. The stresses are the same at the debond tip, as expected; however, the stresses are higher over a longer length for the thicker adherend specimen.

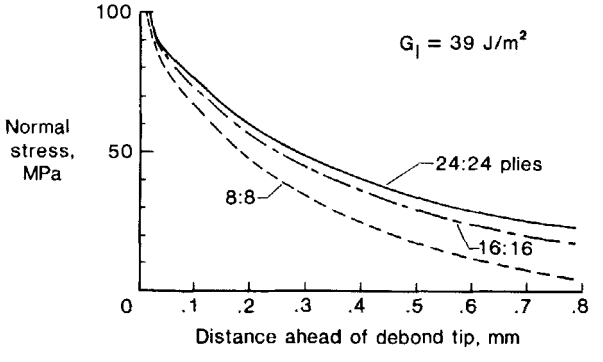

FIGURE 7 Normal stress distribution ahead of debond front.

Figure 5 indicates that the thinner specimens would have lower values of threshold G for cyclic debonding. Since the design of bonded joints may be based on threshold values because of the large values of the exponent n,[13] this effect may become important for thin adherends. An important implication of this result is that a choice of too thick a specimen for measurement of fatigue characteristics may overestimate the threshold G and fatigue life. However, the shift in debond growth rate due to adherend thicknesses is almost within the scatter band of the data.

Shivakumar and Crews[14] have stated that the height of the plastic zone, not the area, is what influences the relative toughness. If this is true, perhaps a thicker adherend may cause high enough stresses to yield the composite matrix material above and below the bondline to a greater extent than a thinner adherend. This possibility was not explored in this study.

The examination of the fracture surfaces of the symmetric DCB specimen (see Figure 8) revealed that the fracture remained mainly in the adhesive showing a cohesive failure of the adhesive material as in Figure 8a. Occasionally, a few fibers were pulled from one surface to the other, particularly, at larger crack lengths (see Figure 8b), but the failure was predominantly in the adhesive.

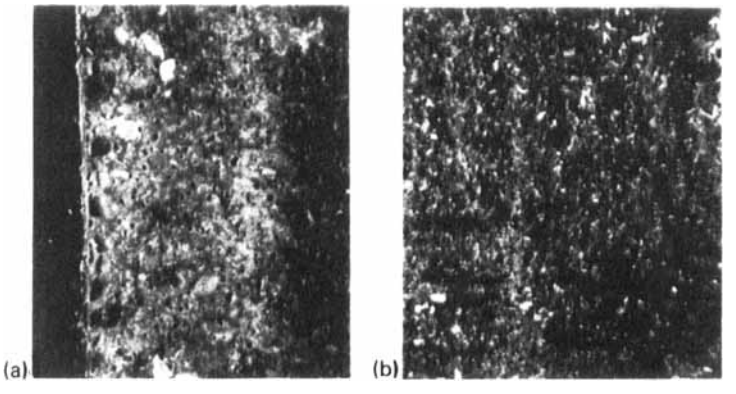

FIGURE 8 Typical failure surfaces of symmetric DCB specimen. (a) Debond surface near the Teflon starter. (b) Debond surface 50 mm away from the Teflon starter. Failure is through the adhesive.

4.4 Influence of the mixed mode

The influence of the mixed mode in a predominantly mode I situation was studied using unsymmetric DCB specimens. Both static fracture toughness and fatigue debond growth rate tests were conducted on 8-ply to 16-ply and 8-ply to 24-ply specimens. These tests showed unexpectedly low fracture toughness values (see Figure 9) and high debond growth rates (see Figure 10a, b). On examination of the fracture surfaces, it was found that the debond in the adhesive quickly migrated to the thinner adherend and propagated as an interfacial failure and further on as delamination in the composite adherend for both the static and fatigue loading. These results are discussed below.

The static fracture toughness values obtained as the debond migrated from the center of the adhesive layer to the interface and further into the adherend as a delamination are shown in Figure 9. There is a continuous reduction in the fracture toughness as the migration of the debond proceeds. The zone in which the failure was fully in the adhesive was very small and at the beginning of the test (near the Teflon starter, see Figure 11a). The transition zone can be seen in Figure 11a only a little distance away from the crack starter. The delamination failure as shown in Figure 11b was seen everywhere else. The low toughness values corresponding to the delamination are somewhat higher than the delamination toughness

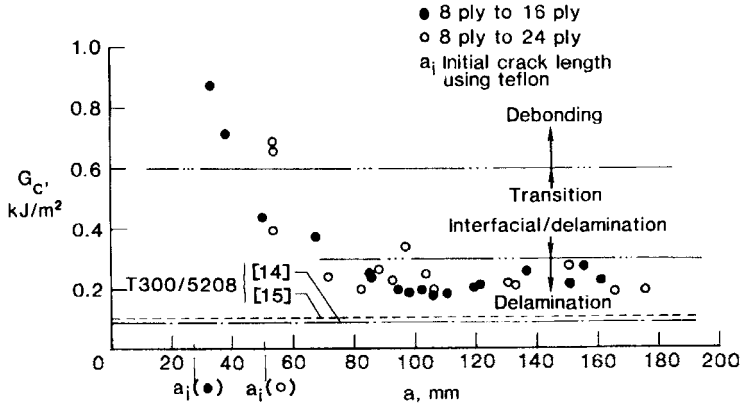

FIGURE 9 Decrease in the fracture toughness with change of failure mode as debond grows in unsymmetric DCB specimen.

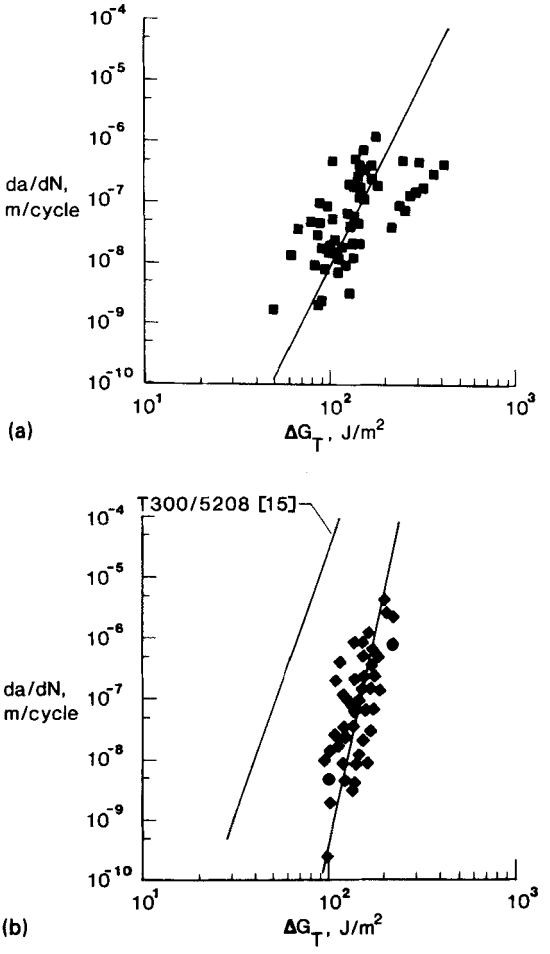

FIGURE 10 (a) Cyclic debond growth in unsymmetric 8-ply to 16-ply DCB specimen. (b) Cyclic debond growth in unsymmetric 8-ply to 24-ply DCB specimen.

values obtained in DCB tests on T300/5208 composites by earlier investigators.[15,16] However, as discussed in Ref. 13, even a small amount of mixed mode is expected to increase the total critical strain energy release rate by a significant amount for a brittle resin like 5208. This is reflected in the higher values of the delamination toughness in the present tests.

High rates of crack growth were obtained in the fatigue tests on the unsymmetric specimens, as seen from Figures 10a,b. Figure 10a shows the cyclic crack growth data for the 8-ply to 16-ply case, and Figure 10b shows the same for the more unsymmetric 8-ply to 24-ply case. It is seen that the more unsymmetric case led to a steeper slope of the best fit line. Figure 10b also shows an earlier result on delamination of T300/5208 unidirectional composite from Ref. 14. Note that the slope of the line in the present case is comparable to the one corresponding to the delamination. The examination of the failure surfaces revealed that in the 8-ply to 24-ply case, the debond migrated to the adherend almost immediately after the start of the test and propagated as delamination (a typical failure surface is shown in Fig. 11b); whereas, in the 8-ply to 16-ply case, the transition to delamination was somewhat more gradual (failure surface as in Figure 11a). Because the debond growth rate data consists of both debonding of EC3445 adhesive and delamination growth in the adherend matrix material 5208, the scatter in the 8-ply to 16-ply data is greater than that in the 8-ply to 24-ply data (see Figures 10a, b). Thus, it is observed that the introduction of asymmetry and mixed mode has caused the debond

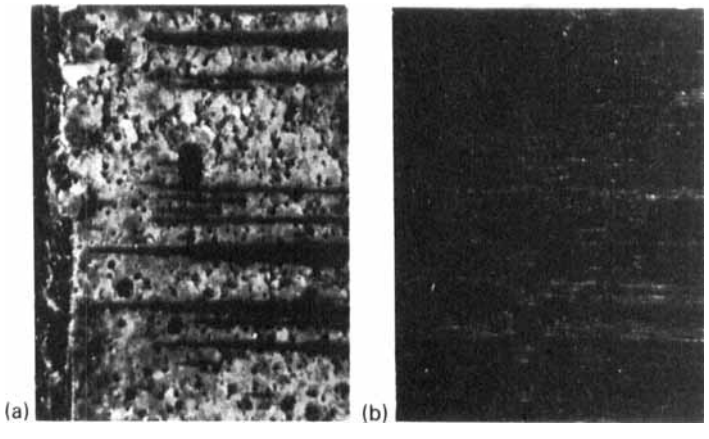

FIGURE 11 Typical failure surfaces of unsymmetric DCB specimens. (a) Fracture surface near the Teflon starter. Failure is primarily in the adhesive layer. (b) Fracture surface 10 mm away from the Teflon starter. Failure is through the graphite-epoxy adherend.

to be pushed to the thinner adherend interface and even inside the composite adherend. This resulted in an undesirable combination of high fatigue growth rates, low fatigue threshold, and low fracture toughness.

It may be noted here that the earlier experiments on the CLS specimens[2,17] of the same adhesive-adherend system with 0-degree plies next to the adhesive showed cohesive failures in the bondline. These CLS specimens also had different adherend thicknesses which resulted in various mixed mode loadings. In the case of CLS specimens, G_I/G_{II} ratios were in the range 0.25–0.31 compared to 5–24 for the unsymmetric DCB specimens. As previously discussed, the symmetric DCB specimens also did not result in delamination of the adherend. The authors cannot explain at this time why a small amount of mode II in the unsymmetric DCB case would cause the debond to wander into the adherend. However, it appears that in the unsymmetric DCB case, the thinner adherend experienced higher bending stresses in the ply next to the adhesive than the thicker adherend; hence, it is more apt to experience fiber failure. The finite element analysis results indicate that the strain in the fiber next to the adhesive approaches 0.01 as the G_I approaches the G_{Ic} of the EC3445 adhesive (850 J/m^2). This, coupled with high interlaminar shear stresses due to the bending, makes the damage more prone to progress into the thinner adherend.

Since the debond wandered into the thinner adherend and continued to grow as a delamination, the debonding behavior of the adhesive under the predominately mode I mixed mode loading could not be evaluated with the present set of specimens.

5 CONCLUSIONS

Symmetric and unsymmetric double cantilever beam (DCB) specimens were tested to investigate the effects of adherend thickness and mixed mode on debond growth in adhesively bonded composite joints in predominantly mode I situations. The tests were conducted under both load and displacement control. The adherends were 8-, 16- and 24-plies thick and made from unidirectional graphite-epoxy (T300/5208) composite. The adhesive was EC3445. Static and fatigue tests were conducted to obtain fracture toughness and

fatigue debond growth rates. The following conclusions were drawn from the present study:

(i) The thickness of the adherend in double cantilever beam specimens influences the measured static fracture toughness of the adhesive. The thicker the adherend the higher the static toughness. The rate of increase in toughness decreases with increasing adherend thickness. The increase in average toughness was less than 20% between 8-ply and 24-ply thick adherends.

(ii) Cyclic debond growth rates are influenced by the adherend thickness. Thicker adherends produce slower debond growth rates. The thickness effects are greatest at low values of strain energy release rate. Thicker adherends result in higher threshold strain energy release rates. The observed adherend thickness effect is much greater for specimens tested in load control than it is in those tested in displacement control.

(iii) The influence of thicker adherends in increasing fracture toughness and lowering crack growth rates appears to be related to the size of the plastic zone (stress distribution) ahead of the debond tip. The plastic zone is longer for thicker adherends. The thicker adherend specimens use a larger percent of the available energy to create the associated larger plastic zone, thereby leaving less energy to propagate the damage. This conclusion is only speculative because there are several unresolved issues.

(iv) Load controlled double cantilever beam tests produced slower debond growth rate data than did the displacement controlled tests. A definite reason for this behavior could not be found. However, it too may be related to the stress distribution ahead of the debond.

(v) The symmetric double cantilever beam specimens produced cohesive debond failures. The unsymmetric double cantilever beam specimens produced debonds that quickly grew to the adhesive/adherend interface then became a delamination in the thinner adherend. Since the 5208 matrix material has lower fracture toughness and higher delamination growth rate than the EC3445 adhesive, this damage migration markedly decreases the damage tolerance of the joint.

(vi) The cyclic debond growth rates data from the symmetric double cantilever beam specimens and cracked lap shear specimens correlated better with G_T than with G_I, supporting the hypothesis

that total strain energy release rate is the governing factor for cyclic debond growth in tough adhesives. The hypothesis could not be tested for the mixed mode unsymmetric double cantilever beam specimen because of the wandering of the damage into the adherend.

Acknowledgement

The first author, P. D. Mangalgiri (National Research Council Resident Research Associate), gratefully acknowledges the support extended by the National Research Council, Washington D.C., through their Associateships Program.

References

1. G. L. Roderick, R. A. Everett Jr. and J. H. Crews, Jr., "Debond Propagation in Composite-Reinforced Metals", *Fatigue of Composite Materials,* ASTM STP 569 (American Society for Testing and Materials, Philadelphia, 1975), pp. 295–306.
2. S. Mall, W. S. Johnson and R. A. Everett, Jr., "Cyclic Debonding of Adhesively Bonded Composites", in *Adhesive Joints,* K. L. Mittal, Ed. (Plenum Press, New York, 1982), pp. 639–658.
3. S. Mall and W. S. Johnson, "Characterisation of Mode I and Mixed Mode Failure of Adhesive Bonds between Composite Adherends", *Composite Materials Testing and Design (Seventh Conference), ASTM STP 893,* J. M. Whitney Ed. (American Society for Testing and Materials, Philadelphia, 1986), pp. 322–334.
4. T. R. Brussat, S. T. Chiu and S. Mostovoy, "Fracture Mechanics for Structural Adhesive Bonds", *AFML-TR-77-163,* Air Force Materials Laboratory, Wright–Patterson AFB, Ohio, U.S.A., 1977.
5. J. Romanko and W. G. Knauss, "Fatigue Behaviour of Adhesively Bonded Joints", *AFWAL-TR-80-4037,* Vol. 1, Air Force Wright Aeronautical Laboratories (Materials Laboratory), Wright–Patterson Air Force Base, Ohio, U.S.A., Apr. 1980.
6. R. A. Everett, Jr., "The Role of Peel Stresses in Cyclic Debonding", *Adhesives Age,* **26,** (5), 24–29 (1983).
7. K. N. Shivakumar and J. H. Crews, Jr., "Bolt Clamp-up Relaxation in a Graphite/Epoxy Laminate", *Long Term Behaviour of Composites, ASTM STP 813,* T. K. O'Brien, Ed. (American Society for Testing and Materials, Philadelphia, 1983), pp. 5–22.
8. G. R. Irwin, "Fracture Mechanics", in *Structural Mechanics,* Goodier and Hoff Eds. (Pergamon Press, New York, 1960), p. 557.
9. D. J. Wilkins, *et al.*, "Characterising Delamination Growth in Graphite-Epoxy", *Damage in Composite Materials: Basic Mechanisms, Accumulation, Tolerence and Characterization, ASTM STP 775,* K. L. Reifsnider Ed. (American Society for Testing and Materials, Philadelphia, 1981), pp. 168–183.
10. M. Ashizawa, "Improving Damage Tolerance of Laminated Composites Through the Use of New Tough Resins", *Proc. Sixth Conf. on Fibrous Composites in Structural Design,* New Orleans, Jan. 1983.

11. B. Dattaguru, R. A. Everett, Jr., J. Whitcomb and W. S. Johnson, *J. Engng. Maths. and Technology*, ASME, **106,** 59–65 (1984).
12. D. F. Devitt, R. A. Schapery and W. L. Bradley, *J. Composite Maths.* **14,** 270 (1980).
13. W. S. Johnson and S. Mall, "A Fracture Mechanics Approach for Designing Adhesively Bonded Joints", in *Delamination and Debonding of Materials,* ASTM STP 876, W. S. Johnson Ed. (American Society for Testing and Materials, Philadelphia, 1985), pp. 189–199.
14. K. N. Shivakumar and J. H. Crews, Jr., "Energy Dissipation Associated with Crack Extension in an Elastic–Plastic Material", *NASA TM 89032,* National Aeronautics and Space Administration, Washington DC, October 1986.
15. W. S. Johnson and P. D. Mangalgiri, "Influence of the Resin on Interlaminar Mixed Mode Fracture", in *Toughened Composites, ASTM STP 937,* N. J. Johnston, Ed. (American Society of Testing and Materials, Philadelphia, 1987), pp. 295–315.
16. R. L. Ramkumar and J. D. Whitcomb, "Characterisation of Mode I and Mixed Mode Delamination Growth in T300/5208 Graphite/Epoxy", in *Delamination and Debonding of Materials, ASTM STP 876,* W. S. Johnson Ed. (American Society for Testing and Materials, Philadelphia, 1985), pp. 315–335.
17. W. S. Johnson and S. Mall, *J. Composites Technology and Research,* ASTM, **8,** 3–7 (1986).